Clim Dyn
DOI 10.1007/s00382-010-0881-4

Daily atmospheric variability in the South American monsoon system

V. Krishnamurthy · Vasubandhu Misra

Received: 21 January 2010 / Accepted: 6 July 2010

Abstract The space–time structure of the daily atmospheric variability in the South American monsoon system has been studied using multichannel singular spectrum analysis of daily outgoing longwave radiation. The three leading eigenmodes are found to have low-frequency variability while four other modes form higher frequency oscillations. The first mode has the same time variability as that of El Nino-Southern Oscillation (ENSO) and exhibits strong correlation with the Pacific sea surface temperature (SST). The second mode varies on a decadal time scale with significant correlation with the Atlantic SST suggesting an association with the Atlantic multidecadal oscillation (AMO). The third mode also has decadal variability but shows an association with the SST of the Pacific decadal oscillation (PDO). The fourth and fifth modes describe an oscillation that has a period of about 165 days and is associated with the North Atlantic oscillation (NAO). The sixth and seventh modes describe an intraseasonal oscillation with a period of 52 days which shows strong relation with the Madden-Julian oscillation. There exists an important difference in the variability of convection between Amazon River Basin (ARB) and central-east South America (CESA). Both regions have similar variations due to ENSO though with higher magnitude in ARB. The AMO-related mode has almost identical variations in the two regions, whereas the PDO-related mode has opposite variations. The interseasonal NAO-related mode also has variations of opposite sign with comparable magnitudes in the two regions. The intraseasonal variability over the CESA is robust while it is very weak over the ARB region. The relative contributions from the low-frequency modes mainly determine the interannual variability of the seasonal mean monsoon although the interseasonal oscillation may contribute in a subtle way during certain years. The intraseasonal variability does not seem to influence the interannual variability in either region.

Keywords South American monsoon · ENSO · Atlantic multidecadal oscillation · Intraseasonal oscillation-MJO · NAO

1 Introduction

The South American monsoon system (SAMS) has been shown to have some similarities with the South Asian summer monsoon (Zhou and Lau 1998; Vera et al. 2006), although the SAMS is weaker in strength and can be identified with the seasonal reversal of low level winds only after the annual mean is removed. The SAMS circulation responds to the strong diabatic heating released in the monsoonal precipitation (Lenters and Cook 1997) which has a distinct annual cycle in certain parts of the continent (Vera et al. 2006). For example, the Bolivian high (an upper level feature) and the Gran Chaco low (a low level feature) are shifted as the season progresses (Zhou and Lau 1998; Grimm et al. 2005).

V. Krishnamurthy (✉)
Center for Ocean-Land-Atmosphere Studies (COLA),
Institute of Global Environment and Society (IGES),
4041 Powder Mill Road, Suite 302, Calverton, MD 20705, USA
e-mail: krishna@cola.iges.org

V. Krishnamurthy
Department of Atmospheric, Oceanic and Earth Sciences,
George Mason University, Fairfax, VA 22030, USA

V. Misra
Department of Meteorology and Center for Ocean-Atmospheric Prediction Studies, Florida State University,
Tallahassee, FL 32306, USA

Published online: 20 July 2010

The austral summer season rainfall in the Amazon Basin is known to be associated with the El Niño-Southern Oscillation (ENSO) variations (Kousky et al. 1984; Aceitunuo 1988; Ropelewski and Halpert 1987; Marengo 1992, 1995; Marengo and Hastenrath 1993; Rao et al. 1996; Fu et al. 2001). The warm (cold) phase of ENSO in the eastern Pacific Ocean coincides with reduced (increased) rainfall in this region. During an El Niño, anomalous ascending motion over the eastern Pacific Ocean under the influence of warm sea surface temperature (SST) is thought to induce anomalous subsidence east of the Andes resulting in below average precipitation in the northern Amazon Basin (Marengo and Hastenrath 1993). However, several studies also suggest that the interannual variance over the Amazon Basin is not completely explained by ENSO (Marengo and Hastenrath 1993; Rao et al. 1996; Dettinger et al. 2000). Rao et al. (1996) showed that increased rainfall over the Amazon Basin is also associated with an increase of moisture transport from the Atlantic Ocean.

On the other hand, the interannual variability of precipitation over southeast Brazil is found to be less influenced by ENSO (Liebmann et al. 2001; Carvalho et al. 2002a; Grimm 2003, 2004). Grimm (2003, 2004) indicated that the influence of ENSO over southeast Brazil is sub-seasonal in nature, attributing it to the competition between the remote ENSO forcing and regional processes that cause abrupt change in the rainfall from 1 month to the other. However, a recent study by Krishnamurthy and Misra (2010) has shown that the interannual variation of the rainfall in the central-east part of the continent (60°W–40°W, 20°S–5°S) is significantly influenced by ENSO variations. Furthermore, it was shown that this ENSO influence is seasonally persistent and not subseasonal in its variability. In a related coupled modeling study, Misra (2008a) showed that the ENSO teleconnection over the Amazon (southeast Brazil) is sensitive (insensitive) to air-sea coupling. In fact, this sensitivity of rainfall variability to air-sea interaction is a feature that is shared by other monsoon systems of the globe (Misra 2008b). The importance of air-sea interaction on the interannual variability of rainfall over southeast Brazil and northern Argentina seems to be more significant in the Atlantic Ocean (Robertson and Mechoso 2000; Doyle and Barros 2002; Robertson et al. 2003; Chaves and Nobre 2004).

The southeast Brazil region is also known for its intraseasonal variability (Nogués-Paegle and Mo 1997; Liebmann et al. 1999; Jones and Carvalho 2002). Nogués-Paegle and Mo (1997) showed alternating wet and dry conditions occurring at intraseasonal scales in the South Atlantic Convergence Zone (SACZ) and over the subtropical plains of South America. These see-saw patterns in outgoing longwave radiation (OLR) were identified as a regional component of a larger oscillatory pattern that is linked to the 30–60 day oscillation in the tropics. In the observational study of Liebmann et al. (1999), it is clearly indicated that the OLR fluctuations with periods less than 90 days show maximum variance over the SACZ region and over southeast Brazil during December-February. They further indicate that a local minimum in intraseasonal variance exists over the southern Amazon Basin where the mean convection is at a maximum. Carvalho et al. (2002b), Jones and Carvalho (2002) also showed reversal of 850 hPa zonal winds at intraseasonal scales over southeast Brazil that was associated with simultaneous changes in precipitation variability.

The above discussion points to a need to investigate the relative roles of low-frequency variability and subseasonal variability of the SAMS. It is also necessary to understand the influences of both the Pacific and Atlantic Oceans as far as the low-frequency variability is concerned. An understanding of the relative roles played by the variations at different time scales has important implication on the long-term prediction of the monsoon. The optimism for long-term prediction stems from a hypothesis of Charney and Shukla (1981) according to which the tropical climate variability is mainly determined by slowly varying components such as SST, soil moisture and snow cover. Support for this hypothesis was provided by Krishnamurthy and Shukla (2007, 2008) who analyzed daily rainfall and convection over the South Asian monsoon region and showed the existence of seasonally persisting signals along with intraseasonal oscillations of different periods. The seasonally persisting components were shown to be related to the SSTs of ENSO and Indian Ocean dipole (IOD) mode (Krishnamurthy and Kirtman 2009). The interannual variability of the seasonal mean rainfall is mainly determined by the relative contributions from the ENSO and IOD related signals. However, the oscillations are important in the subseasonal variability and may contribute in a small way to the seasonal mean during certain years when the influence of SST is weak.

The purpose of this study is to perform a similar analysis of the SAMS in order to identify the components of variability on different time scales, to obtain their space–time structures and to determine their relative roles in the intraseasonal and interannual variability of the atmosphere over South America. More specifically, the objective of this study is to provide observational evidence for the relative roles of slowly varying components that are related to SST variability and high-frequency components that vary on intraseasonal time scale. The relation to the SSTs of both the Pacific and Atlantic Oceans will be investigated. The relative contributions of these various components in determining the interannual variability of the seasonal mean monsoon will be analyzed. The regional

variations of the influence of components of different time scales will also be examined by separately analyzing the variability over the Amazon Basin and the central-east part of South America. The objectives of this study are achieved by performing multichannel singular spectrum analysis (MSSA) of daily observed OLR anomalies over South America and the adjoining oceanic region. This method allows the decomposition of the total variability into nonlinear oscillations, persisting signals and trends and to study their space–time structures on a daily time scale basis. This study may be considered as an expansion of our earlier work (Krishnamurthy and Misra 2010), which primarily dwelled on the ENSO-forced variability over central-east South America. This paper examines the variations over central-east South America and the Amazon River Basin at decadal and intraseasonal time scales also. This study also includes the forcing from the Atlantic SST variation and provides a comparison with the ENSO-forced variability.

In Sect. 2, the data and method of analysis are described. The climatologies of OLR and precipitation are discussed in Sect. 3. The results of the MSSA of daily OLR anomalies are given in Sect. 4. Section 5 discusses the low-frequency modes while Sect. 6 describes the higher frequency modes. A final discussion of the results is given in Sect. 7.

2 Data and method of analysis

The analysis of daily variability in this study uses observed outgoing longwave radiation which represents deep convection. Daily mean values of OLR for the period 1979–2007 on 2.5° longitude × 2.5° latitude grid were obtained from the National Oceanic and Atmospheric Administration (NOAA, Liebmann and Smith 1996). The data prior to 1979 were not used because of discontinuity in 1978 caused by satellite problems. The one-degree daily precipitation data set developed by the Global Precipitation Climatology Project (GPCP, Huffman et al. 2001) has also been used for the period 1997–2007. To study the relation with SST, the newly developed optimally interpolated SST (OISST Version 2) data set (Reynolds et al. 2007) from NOAA was obtained for the period 1982–2007. The daily values of SST are available on 0.25° × 0.25° grid. The dynamical fields which are analyzed include daily mean horizontal winds at 850 and 200 hPa and mean sea level pressure (MSLP) for the period 1979–2007 extracted from the National Centers for Environmental Prediction (NCEP) Reanalysis-2 dataset (Kanamitsu et al. 2002). The daily climatology was computed as the mean for each calendar day, and was subtracted from the total field to obtain the daily anomalies.

The main method of analysis extracts the space–time structure of the atmospheric variability by performing multi-channel singular spectrum analysis of the daily OLR anomalies over the South American monsoon region. The MSSA is applied to obtain oscillatory and persistent modes by following the mathematical formulation described by Ghil et al. (2002). This method has been used in studies on Indian monsoon to understand the intreaseasonal oscillations and low-frequency persistent signals (Krishnamurthy and Shukla 2007, 2008). For data specified at L grid points and N discrete times, the MSSA is applied to 0 to $M - 1$ lagged copies of the data which results in LM eigenvalues and LM eigenvectors. Each eigenvalue provides the variance explained by the corresponding eigenmode. The eigenvectors, each containing a sequence of M maps on L grid points, are the space–time empirical orthogonal functions (ST-EOF). Each eigenmode also has a space–time principal component (ST-PC) of time length $N - M + 1$. The original data can be expressed as the sum of all the reconstructed components (RCs) formed from the corresponding ST-EOFs and ST-PCs. Each RC, corresponding to a particular eigenmode, is a time series of maps with the same grid and same time length as the original time series. The RCs are considered as filtered data obtained by data-adaptive method.

3 Climatology

The mean climate over South America is shown as annual climatological mean OLR for the period 1979–2007 in Fig. 1a. Most of the northern part (north of 20°S), which includes part of the Amazon River basin, is covered with OLR less than 220 W m^{-2} indicating strong convection. The northwest region consists of a large area with maximum convective activity. Over much of the southern part (40°S–20°S) of the continent and the eastern part of Brazil, the mean OLR is in the range 230–260 W m^{-2}. The equatorial eastern Pacific and Atlantic Oceans are regions of less convective activity with OLR ranging from 250 to 270 W m^{-2}. However, the South Atlantic Convergence Zone (SACZ) shows moderate convective activity. An examination of the climatological mean OLR for the December-January-February-March (DJFM) season (figure not shown) showed a pattern similar to that of the annual mean (Fig. 1a) but with more intense convection (190–225 W m^{-2}) in the northern part of the continent and slightly higher values of OLR elsewhere including the oceanic regions.

The standard deviation of daily OLR anomalies for all days of the period 1979–2007 is plotted in Fig. 1b which shows values in the range of 25–40 W m^{-2} over most of the continent and in the oceanic region of SACZ. The

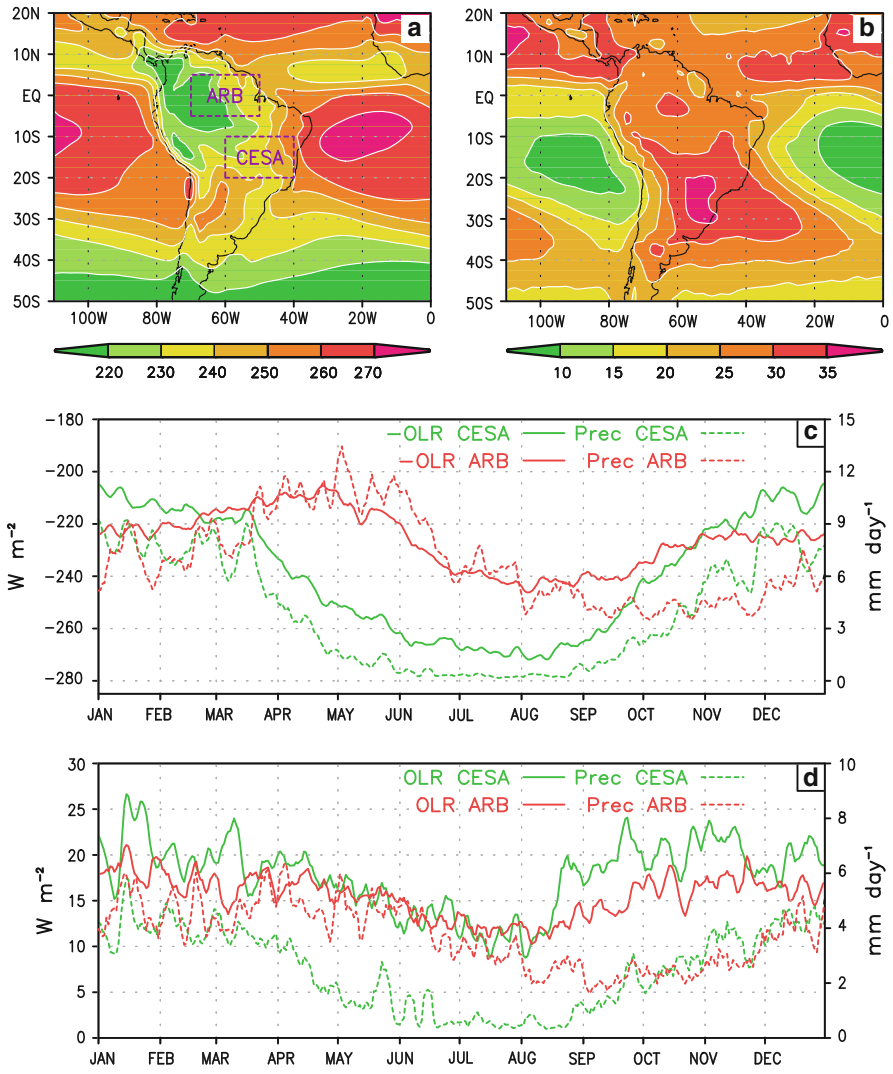

Fig. 1 **a** Annual climatological mean and **b** standard deviation of daily OLR anomalies. **c** Annual cycles of daily climatological mean OLR (*solid green*) and precipitation (*dashed green*) averaged over CESA region and annual cycles of daily climatological mean OLR (*solid red*) and precipitation (*dashed red*) averaged over ARB region. The OLR averages are plotted with their negative values for easy comparison with the precipitation. **d** Annual cycles of daily standard deviation of OLR (*solid green*) and precipitation (*dashed green*) anomalies averaged over CESA region and annual cycles of daily standard deviation of OLR (*solid red*) and precipitation (*dashed red*) averaged over ARB region. The climatological means and standard deviations are based on the period 1979–2007 for OLR and on 1998–2008 for precipitation. The domains of CESA (60°W–40°W, 20°S–10°S) and ARB (70°W–50°W, 5°S–5°N) are shown as dashed boxes in (**a**). In (**c**) and (**d**), the scales for OLR are shown on the left and those for precipitation on the *right*. The units of OLR and precipitation are W m^{-2} and mm day^{-1}, respectively

standard deviation is uniform with slightly lower value in the northern part of the continent compared to the region south of 15°S. The regions of least convective activity in the Pacific and Atlantic Oceans (Fig. 1a) also have the lowest daily variability (Fig. 1b). The daily standard deviation of OLR was also examined for just the DJFM season (figure not shown) and found to be quite similar to the all season variability shown in Fig. 1b but with values higher by 5–10 W m^{-2}.

In order to study the difference in the convection between the northern and central parts of South America, the region (70°W–50°W, 5°S–5°N), referred to as the Amazon River Basin (ARB), and the region (60°W–40°W, 20°S–10°S), referred to as the central-east South America (CESA), are selected. The CESA region in this study is slightly different from that defined by Krishnamurthy and Misra (2010) so that the two regions are of same size and not overlapping. The area averages of any variable over these two regions will be called the ARB index and CESA index. The annual cycles of daily ARB and CESA indexes of OLR and their daily standard deviations are shown in Fig. 1c, d, respectively. For more support, the annual cycles of precipitation using GPCP data for the period 1998–2007 are also shown. The annual cycle of CESA index is more robust with a well-defined dry season with no precipitation (280 W m^{-2} OLR) during June-July-August-September (JJAS) and a well-defined wet season with 6–9 mm day^{-1} precipitation (200–220 W m^{-2} OLR) during DJFM (Fig. 1c). On the other hand, the annual cycle of ARB index does not reveal well-defined wet and dry seasons corresponding to the austral summer and winter seasons, respectively. The ARB index is in the range of 4–11 mm day^{-1} precipitation (210–240 W m^{-2} OLR) with maximum during April-June and minimum during September–November. Although the ARB and CESA indexes are close during DJFM, they differ by

6–9 mm day^{-1} in precipitation (200–220 W m^{-2} in OLR) during May–September.

The standard deviation of the CESA index also has a stronger annual cycle compared to the ARB index (Fig. 1d), and both reveal the same seasonal characteristics as those of the daily mean (Fig. 1c). The standard deviation of the CESA reaches up to 4 mm day^{-1} in precipitation (25 W m^{-2} in OLR) whereas the standard deviation of the ARB index has a maximum of 6 mm day^{-1} in precipitation (20 W m^{-2} in OLR). Generally, the variability of convection is higher in the CESA region than in the ARB region although not in the precipitation.

4 MSSA of daily OLR anomalies

The space–time structure of the variability of convection over the South American monsoon region was obtained by applying MSSA to daily OLR anomalies in (110°W–0°, 50°S–20°N) region for all the days of the period 1979–2007. A lag window of 121 days at 1 day interval was used. The eigenmodes obtained from MSSA are arranged in descending order of the variance explained. The first seven eigenmodes are found to consist of three non-oscillatory modes with low-frequency variability and two pairs of oscillatory modes of different periods. These seven modes describe important features of the South American monsoon system varying from intraseasonal to decadal time scales, while the rest of the modes are in time scales of higher frequency. Therefore, this paper will discuss only the first seven eigenmodes. The variance explained ranges from 0.9% for the first mode to 0.3% for the seventh mode. These values are small because of the fact that the MSSA has been applied to raw daily anomalies without pre-filtering in order to obtain space–time modes in a data-adaptive manner. The important point to note is that these are the leading modes while the other modes have even less variance and progressively become indistinguishable from noise. The same seven modes were also obtained when the MSSA procedure was repeated with 5 and 15-day running means of daily OLR anomalies but now with 2.0, 4.4% for the first mode and 0.7, 1.2% for the seventh mode, respectively. The MSSA eigenmodes of raw anomalies are used in further discussion.

Since the length of the lag window is 121 days, each MSSA mode consists of an ST-EOF which is a sequence of 121 lagged maps and an ST-PC whose time length is equal to the number of days in the period 1979–2007 minus 120 days. The ST-EOF and ST-PC are used to construct the space–time RC of each eigenmode (see Ghil et al. 2002). The RCs are on the same spatial grid and have the same time length and sequence as the original data. An examination of the ST-EOF, ST-PC and RC of each eigenmode, following the criteria specified by Ghil et al. (2002), the eigenmodes 1, 2 and 3 were found to be non-oscillatory at low-frequency time scales and modes (6, 7) to be an oscillatory pair with 52-day period. The modes (4, 5) showed all indications of being an oscillation but with a period longer than the length of the lag window. Therefore, a second MSSA was performed on just the RC of mode (4, 5) with a longer lag window to extract an oscillatory pair with a period of 165 days. The RC of an oscillation is the sum of the RCs of the individual modes of the pair. The RCs of eigenmodes 1, 2, 3, (4, 5) and (6, 7) will be denoted as RC1, RC2, RC3, RC45 and RC67, respectively.

The spatial structure and temporal variation of an RC can be described in a compact manner by performing a spatial EOF analysis of the RC. Since the RCs are coherent modes, the first EOF (EOF1) explains a very high variance (usually above 95%) of the corresponding RC (and not of the total anomaly). The EOF1s of the RCs are shown in Fig. 2 and the corresponding first PCs (PC1s) in Fig. 3. These PCs have the same time length as that of the RCs and hence of the total anomaly, and should not be confused with the ST-PCs of MSSA. The power spectra of the PCs of Fig. 3 are plotted in Fig. 4.

The EOF1 of RC1 (Fig. 2a) shows an east–west structure above 20°S with anomalies of one sign over the continent and equatorial Atlantic Ocean and anomalies of opposite sign over the Pacific Ocean. A north–south structure of opposite anomalies is also seen with the sign changing at 20°S. This structure varies on a daily basis according to the PC1 of RC1 shown in Fig. 3a. The variability of the PC is seen to be mainly interannual without the presence of high-frequency fluctuations. The power spectrum of RC1 (Fig. 4a) is broad-band with a well defined peak at about 45 months which is about the same as that of ENSO. In fact, the variation of PC1 of RC1 is similar to the ENSO variation with warm events of 1982–1983, 1987–1988 and 1997–1998 prominently captured (Fig. 3a). This first MSSA mode is the same as that described by Krishnamurthy and Misra (2010). This study will later discuss further properties of this mode.

While the variability of the first MSSA eigenmode is interannual, the second and third eigenmodes seem to display variation on even longer time scale. For the second mode, the EOF1 of RC2 in Fig. 2b shows anomalies of same sign over the entire continent with maximum values along the elevated region in the southwest. Although the anomalies over the eastern Pacific and Southern Atlantic Oceans are uniformly the weakest, it is important to note that the anomalies over the continent extend over to northern Atlantic Ocean and West Africa. The signal is thus not restricted to land areas only. The PC1 of RC2 (Fig. 3b) indicates variability on decadal time scale with small amplitude interannual variability superimposed. The

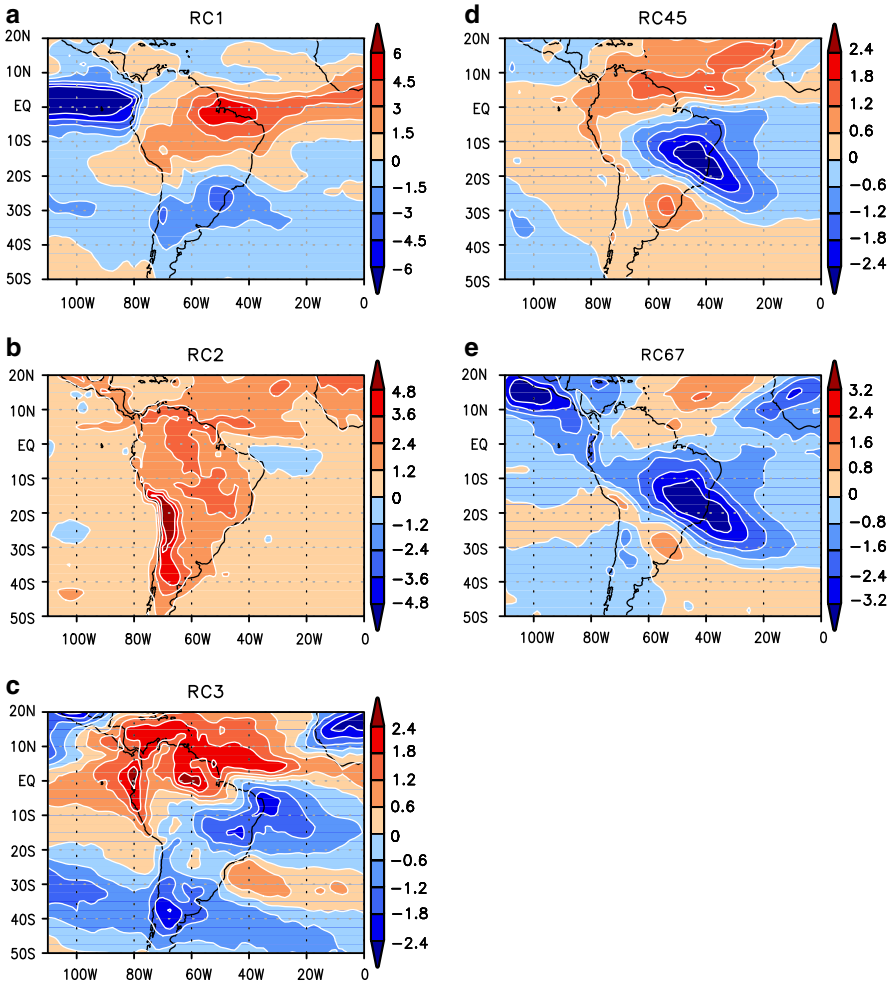

Fig. 2 Spatial EOF1 of the reconstructed components **a** RC1, **b** RC2, **c** RC3, **d** RC45 and **e** RC67 from MSSA of the daily OLR anomalies. The Spatial EOF analysis was performed on the daily values of the RCs for the period 1979–2007. Units are in W m^{-2}

power spectrum of RC2 shown in Fig. 4a is mainly red confirming that the variability is mostly in low-frequency range which is beyond the ENSO band. The EOF1 of RC3 in Fig. 2c shows that the third mode has stronger anomalies of one sign over the northwest part of the continent which extends into the Pacific and Atlantic Oceans while opposite sign anomalies over the continent to the south of 10°S, southern Pacific Ocean and much of Atlantic Ocean south of the equator (except for 25°S–35°S). The PC1 of RC3 (Fig. 3c) also seems to have low-frequency variability which is confirmed by its spectrum (Fig. 4a) which is somewhat red in nature without any peaks.

The spatial structure of the oscillatory pair of eigenmodes (4, 5), as shown by EOF1 of RC45 in Fig. 2d, consists of strong anomalies of one sign over the eastern part of South America and SACZ and weaker anomalies of opposite sign to the south and north. The time variability of PC1 of RC45 (Fig. 3d) shows a nonlinear oscillation whose amplitude, phase and frequency are modulated. From Fig. 4b, the power spectrum of RC 45 reveals a peak at 165-day period. Because of its time scale, the (4, 5) mode will be referred as interseasonal oscillation, hereafter. The second oscillatory pair (6, 7) also has a tilted structure with strong anomalies over the SACZ and extending northwestward onto the Pacific Ocean, as seen from EOF1 of RC67 in Fig. 2e. From PC1 of RC67 in Fig. 3e, this mode is also found to be a nonlinear oscillation but with higher frequency. The power spectrum of RC67 (Fig. 4b) shows that this oscillation has a peak in the intraseasonal time scale at 52 days, similar to Madden-Julian Oscillation (MJO).

5 Low-frequency modes

5.1 Relation with ENSO and decadal oscillations

The association of the first three low-frequency modes with ENSO and decadal phenomena such as the Pacific Decadal Oscillation (PDO) and Atlantic Multidecadal Oscillation (AMO) was investigated. For this purpose, the correlations between the PC1 (in Fig. 3a–c) of the three RCs with daily

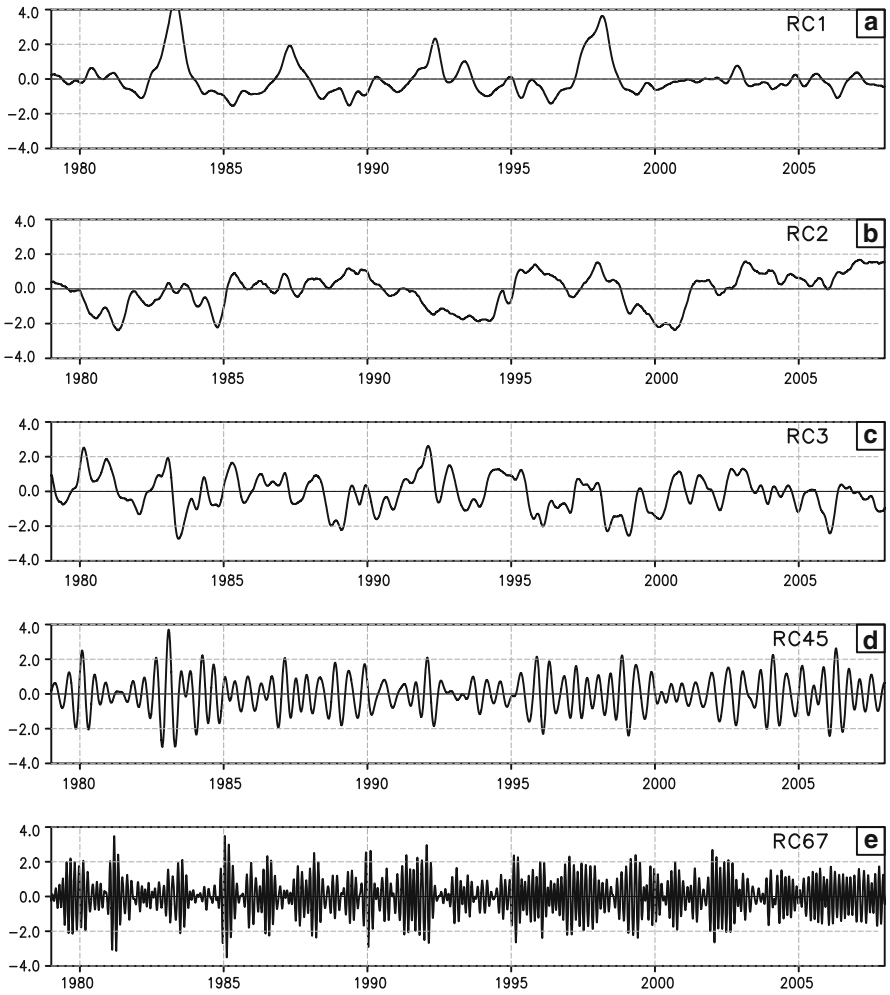

Fig. 3 Spatial PC1 of **a** RC1, **b** RC2, **c** RC3, **d** RC45 and **e** RC67 corresponding to the EOFs shown in Fig. 2. The PCs are divided by their respective standard deviations

anomalies of SST (from OISST2) for the period 1982–2007 were computed. Additionally, in order to find the relation with the atmospheric circulation, daily zonal wind (u) anomalies at 850 hPa (from Reanalysis-2) were regressed on PC1 of the RCs.

The point correlation of RC1 with SST, shown in Fig. 5a, clearly reveals the ENSO signature with strong positive correlation in the eastern and central equatorial Pacific Ocean which is surrounded by the familiar horseshoe pattern of negative correlation. These correlations are even stronger in the Pacific Ocean for the DJFM season, as shown by Krishnamurthy and Misra (2010). The regression of the zonal wind field at 850 hPa on RC1 shown in Fig. 5b is consistent with the SST correlation. In the eastern and central equatorial Pacific Ocean, the wind anomalies are westerlies, the effect of which will be to weaken the trade winds and the Walker circulation.

The point correlation of RC2 with SST is shown in Fig. 5c. Significant correlations (reaching up to 0.4) appear in the North Atlantic Ocean, similar to the correlation of the AMO index with the SST anomalies obtained by Knight et al. (2005). The fact that the Atlantic correlation shown in Fig. 5c was obtained by daily correlation with unsmoothed signal (PC of RC2 in Fig. 3b) is noteworthy. The regression of the 850 hPa zonal wind (Fig. 5d) indicates westerly anomalies from equator to 40°N and easterlies in the northern part of the Atlantic Ocean. These relations and the low-frequency temporal variability of RC2 suggest that the second mode is possibly associated with the AMO.

For the third mode, the point correlation of RC3 with SST (Fig. 5e) shows an ENSO-like structure in the Pacific Ocean. However, the correlations, while significant, have moderate values, and the region of maximum correlation is located in the central Pacific Ocean rather than in the eastern Pacific like in the case of RC1. The correlation of same sign extends along the west coast of United States. Corresponding to the warm anomalies in the central Pacific Ocean (Fig. 5e), the regressed 850 hPa zonal wind field in Fig. 5f has strong westerlies. These SST and wind patterns are quite similar to those related to the PDO (Mantua et al.

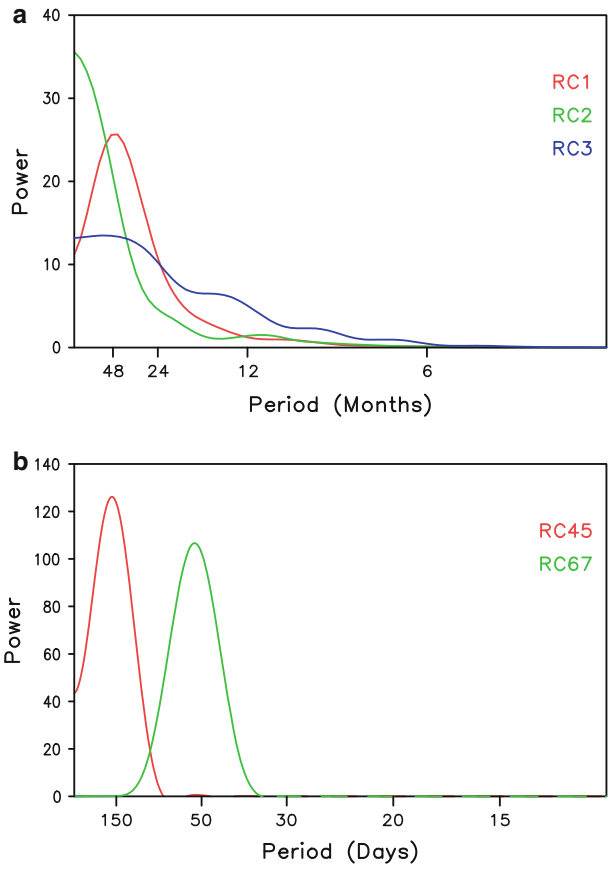

Fig. 4 Power spectra of PC1 (shown in Fig. 3) of **a** RC1 (*red*), RC2 (*green*), RC3 (*blue*), and **b** RC45 (*red*) and RC67 (*green*). The scale of the *x*-axis is in months for (**a**) and days for (**b**)

1997). Again, considering that these are daily correlations and regressions obtained from unsmoothed RC, the result is remarkable. These results and the low-frequency temporal variability of RC3 suggest that the third mode may be associated with the PDO.

5.2 Regional variation

It was noted in Sect. 3 that there are differences in the seasonal climatological mean and annual cycles of daily mean of OLR and precipitation between ARB and CESA regions. Whether such differences also exist in the daily variability is now discussed. The daily values of ARB and CESA indexes of RC1, RC2 and RC3 are shown as time series in Fig. 6 for the period 1979–2007. Figure 6a shows that both ARB and CESA indexes capture the ENSO variability. However, although they are in phase with each other, the amplitude of the ARB index is higher, especially during strong El Niño events.

In the case of RC2, both ARB and CESA indexes have almost identical values all the time (Fig. 6b). This is consistent with the EOF of RC2 (Fig. 2b) which has uniform spatial structure over most of the continent. The ARB and CESA indexes of RC3, however, vary with opposite phases with almost equal amplitude. The different behaviors of the three modes have important regional implication on the interannual and decadal variability of the South American monsoon. Since the RCs are simply added to get the combined variability, the ARB and CESA region could behave differently depending on how the amplitudes and phases of the RCs add up. This point is further examined by considering the seasonal means of the RCs.

In Fig. 7, the interannual variability of the DJFM seasonal means of the RCs are compared by plotting the ARB and CESA indexes. The variability of the ARB index of RC1 follows that of ENSO with major El Niño (1982–1983, 1986–1987, 1991–1992 and 1997–1998) and La Niña (1984–1985, 1988–1989, 1998–1999 and 1999–2000) events being dominant (Fig. 7a). The CESA index of RC1 also has similar ENSO variability but with reduced values (Fig. 7b), generally about one-third the value of ARB index. Interestingly, the 1994–1995 and 2002–2003 El Niño events did not have much effect on ARB and CESA regions. Both ARB and CESA indexes of RC2, which was suggested to be associated with AMO, have almost identical values with intense convection occurring during 1980–1981, 1991–1994, 1998–2001. For RC3, which seems to be related to PDO, the ARB and CESA indexes vary with opposite signs but with comparable magnitudes.

The three leading MSSA modes play a dominant role in determining the interannual variability of the seasonal mean convection or rainfall. During a particular year, the relative values of RC1, RC2 and RC3 determine the seasonal mean convection. From the earlier discussion of Fig. 7a, b, it is clear that the relative contributions of the three modes could be different for ARB and CESA index in a particular year. In order to examine the combined variability, the ARB and CESA indexes were computed for the sum of RC1, RC2 and RC3 (RC123 hereafter). The DJFM seasonal means of the two indexes of RC123 are shown in Fig. 7c. The variability of the ARB index is still predominantly determined by ENSO. However, RC2 is the major factor in certain years such as 1992–1993 and 1998–1999 and RC3 is important in years such as 1988, 1991 and 2005. For the CESA index, the relative values of the three modes appear to be more crucial because of the smaller magnitude of the ENSO mode (RC1) and the opposite sign of the PDO mode (RC3). Although the CESA index still captures the effect of ENSO during 1982, 1984, 1986 and 1997 similar to the ARB index, the ENSO effect is counteracted by other modes in 1988 and 1991 (Fig. 7c).

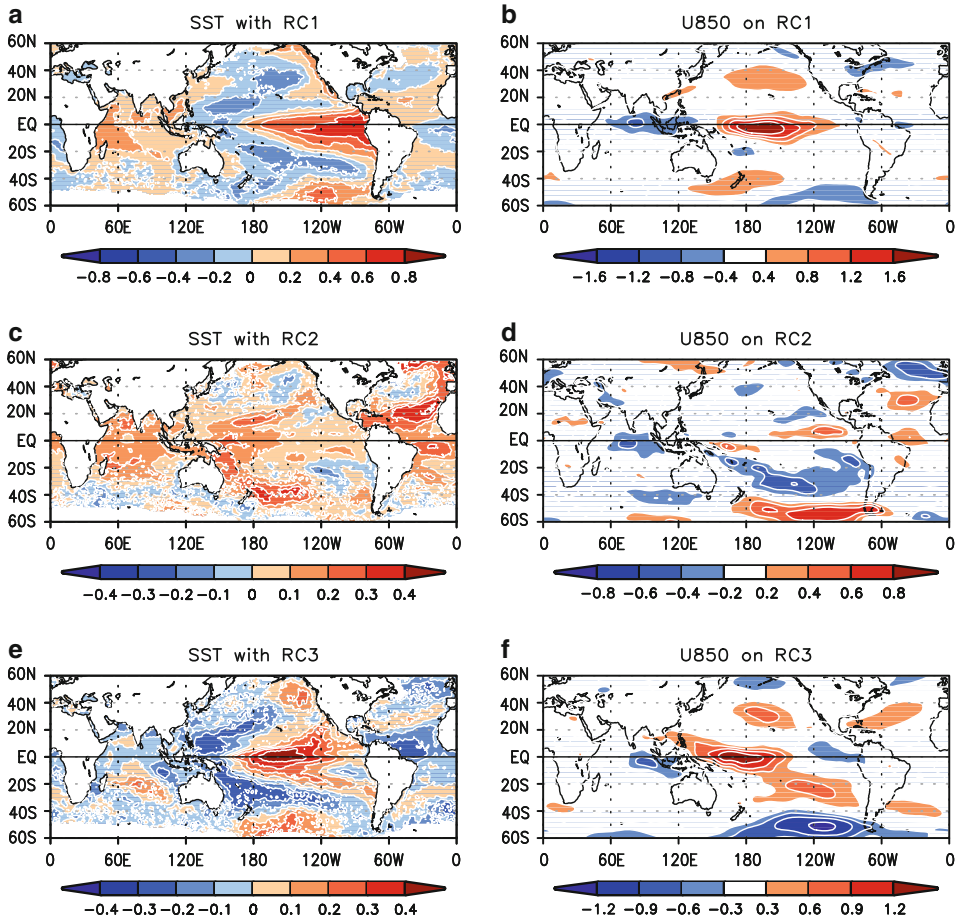

Fig. 5 Simultaneous point correlation of daily PC1 (shown in Fig. 3) of **a** RC1, **c** RC2 and, **e** RC3 of OLR with daily SST anomalies during 1982–2007. Simultaneous regression of zonal wind *u* at 850 hPa on daily PC1 (shown in Fig. 3) on **b** RC1, **d** RC2 and **f** RC3 of OLR for the period 1979–2007. The scale for the contours is shown by the *color bar* below each panel

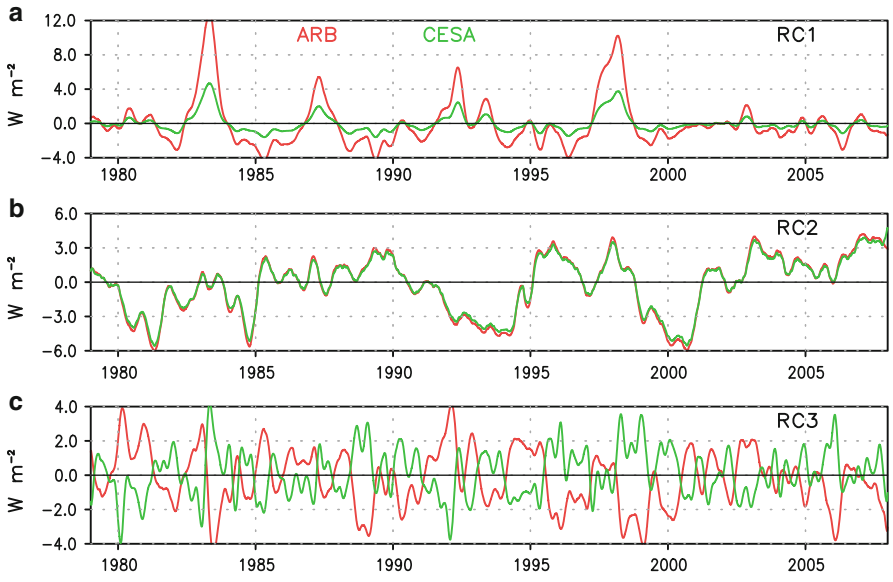

Fig. 6 Time series of ARB and CESA indexes of daily **a** RC1, **b** RC2 and **c** RC3

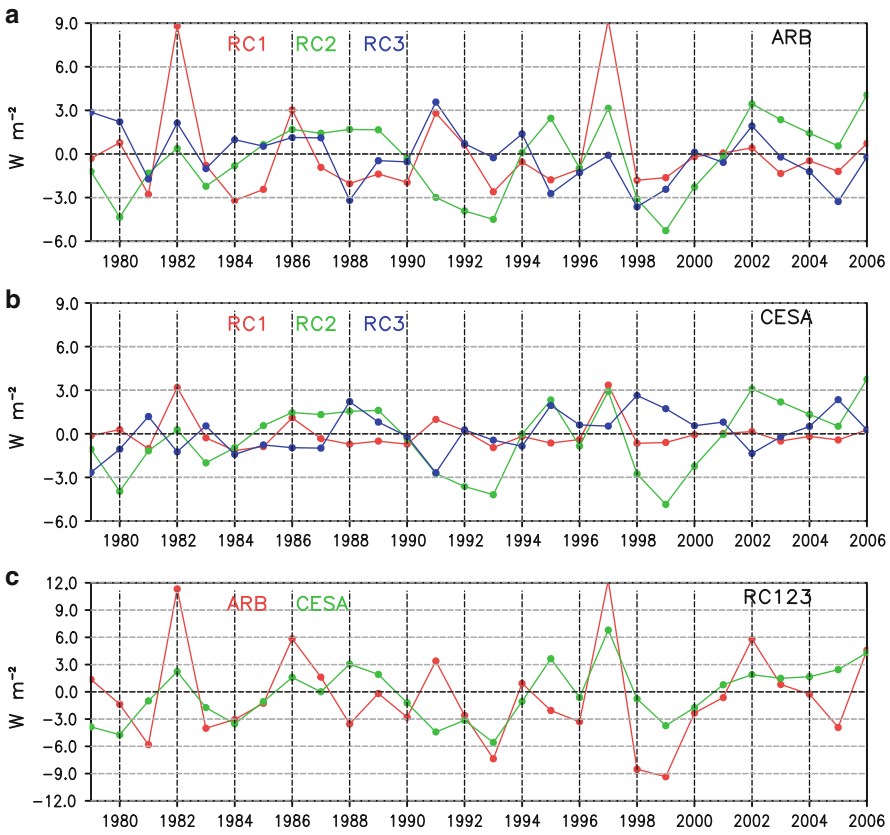

Fig. 7 Time series of **a** ARB and **b** CESA indexes of DJFM seasonal mean RC1 (*red*), RC2 (*green*), RC3 (*blue*). **c** Time series of ARB index (*red*) and CESA (*green*) of DJFM seasonal mean of RC1 + RC2 + RC3

6 Interseasonal and intraseasonal oscillations

The space–time structures of the oscillatory modes at interseasonal and intraseasonal time scales are further discussed in this section. Their association with known phenomena such as the North Atlantic Oscillation (NAO) and MJO is also established.

6.1 Space–time structure and propagation

The amplitude $A(t)$ and phase angle $\theta(t)$ of each of these nonlinear oscillations are determined from the respective RC following the method suggested by Moron et al. (1998). This method has been used in the study of the Indian monsoon by Krishnamurthy and Shukla (2007, 2008). During each cycle of the oscillation, the phase angle $\theta(t)$ varies from 0 to 2π. The space–time structure of the oscillation can be best summarized by constructing composites of the RC based on the phase of the oscillation. A complete phase cycle $(0, 2\pi)$ is divided into eight equal intervals of length $\pi/4$. By averaging the RC of the oscillation in each phase interval for the entire period, eight phase composites of RC are obtained.

For the interseasonal oscillatory mode (4, 5) with a spectral peak centered at 165 days (as discussed in Sect. 4), the composites of RC45 for eight phase intervals in an oscillatory cycle were constructed. The phase composites of RC45, presented in Fig. 8a, represent the average oscillatory cycle during 1979–2007. The period of the average oscillation in Fig. 8a is 165 days, although individual oscillatory cycles, being nonlinear, may have periods greater than or less than 165 days. This variation in the period is reflected in the broadness of the power spectrum of RC45 shown in Fig. 4b. The first four composites are almost exactly the same as the last four with opposite sign. In the second half of the cycle, convective anomalies develop over the SACZ region at about 20°S (phase 5), intensify and move northeastward (phases 6–7) and weaken (phase 8). At the same time, positive anomalies exist in northern region and equatorial Atlantic Ocean. Moreover, another positive anomaly center develops off the South Atlantic coast (around 30°S) which extends northward and replaces the receding negative anomalies. The same sequence but with suppressed convection (positive anomalies) in the SACZ region occurs in phases 1–4. The propagation features of the oscillation are found by examining the Hovmöller diagrams of RC45. Using the phase of the oscillation as time coordinate, the longitude-phase cross section of RC45 composite averaged over (20°S–15°S) is shown in Fig. 9a. The oscillation exhibits

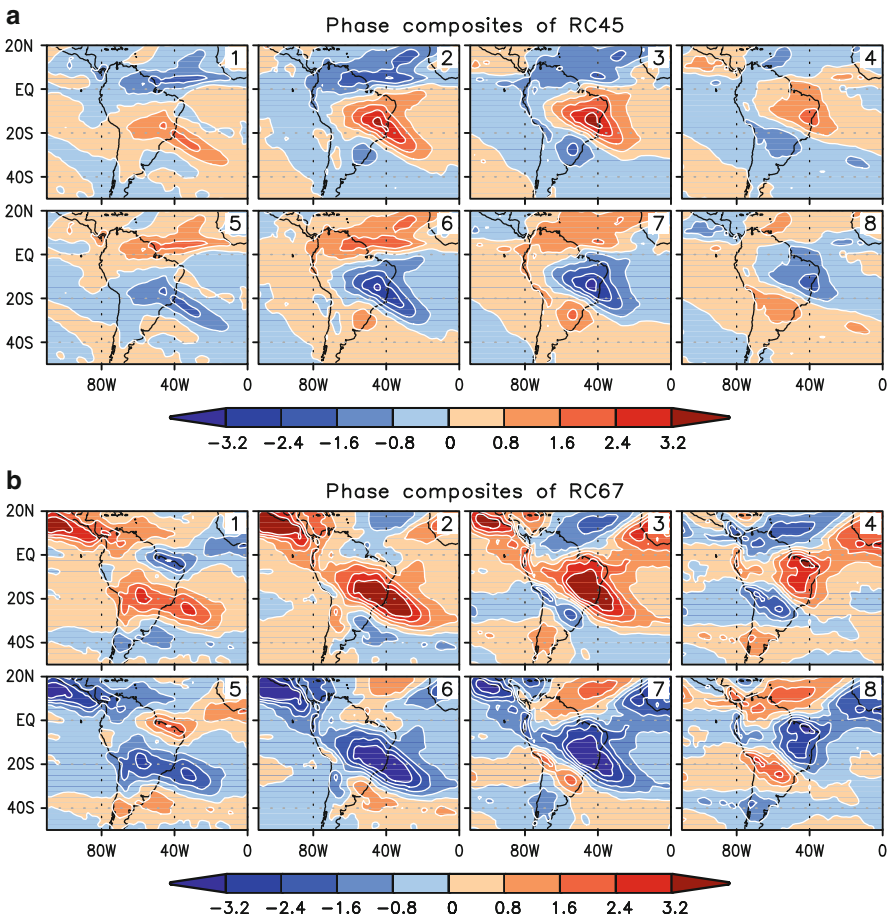

Fig. 8 Phase composites of daily **a** RC45 and **b** RC67 corresponding to eight phase intervals of the respective oscillatory mode during 1979–2007. Units are in W m^{-2}. The phase interval number is given at the top right corner of each panel

eastward propagation limited to 60°W–20°W. The latitude-phase cross-section of RC45 averaged over (60°W–50°W) shows northward propagation between 30°S and 20°N (Fig. 9b).

For the intraseasonal oscillatory mode (6, 7), the phase composites of RC67 in eight phase intervals are plotted in Fig. 8b. The average period of this oscillation is 52 days. In the second half of the cycle in Fig. 8b, moderate convection anomalies appear around 20S in phase 5, intensify and expand in the peak phases 6 and 7. During these phases, the convection zone is aligned along the SACZ and is accompanied by similar anomalies extending into the Pacific beyond the northwest part of the continent. The convection moves to the northeast and diminishes in intensity in phase 8. A similar sequence with positive anomalies occurs in phases 1–4. The magnitude of the anomalies in the intraseasonal oscillation (Fig. 8b) is larger than that in the interseasonal oscillation (Fig. 8a). In the longitude-phase cross section of RC67 composite (Fig. 9c), the evidence for eastward propagation is weak. However, the latitude-phase cross section of RC67 in Fig. 9d shows a clear northward propagation between 30°S and equator.

6.2 Relation with NAO and MJO

Both the interseasonal and intraseasonal oscillations do not have any significant relation with the SST. The point correlation of PC1 of RC45 (the PC shown in Fig. 3d) with the daily SST anomalies of 1982–2007 is shown in Fig. 10a. The correlation is very weak, with maximum values of about −0.2 and 0.2 appearing in the oceanic regions adjoining the continent. Similar point correlation of PC1 of RC67 shows almost no correlation with the SST (Fig. 10b). It is important to note that the lack of correlation is specifically for the two oscillations on daily time scale. The relation between the Atlantic SST and the precipitation in the subtropical region, discussed by Doyle and Barros (2002), is based on the interannual variability of the total precipitation anomalies and not on the daily variability of intraseasonal and interseasonal oscillations. However, possible associations of the interseasonal oscillation with the NAO and the intraseasonal oscillation with the MJO are explored in this section.

The relation between the interseasonal oscillation and other atmospheric variables was analyzed by constructing

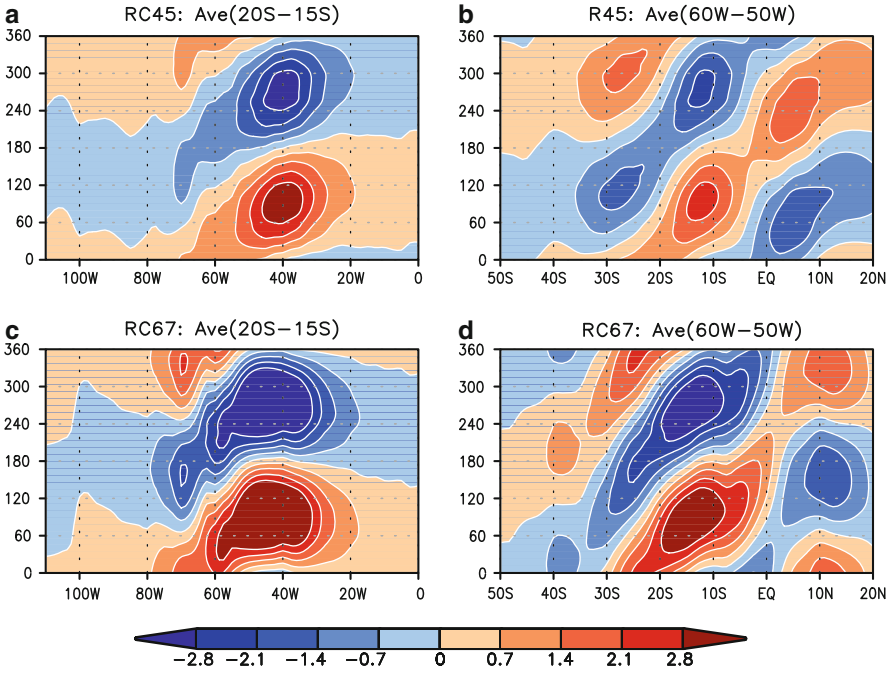

Fig. 9 Hovmöller diagrams of the phase composites of RCs for a complete cycle of 0°–360° phase of the respective oscillatory mode: longitude-time cross-sections of **a** RC45 and **c** RC67 averaged over (20°S–15°S) and latitude-time cross-sections of **b** RC45 and **d** RC67 averaged over (60°W–50°W). Time is represented by the phase of the oscillation. The composites were constructed at intervals of $\pi/12$ for the period 1979–2007. Units are in W m^{-2}

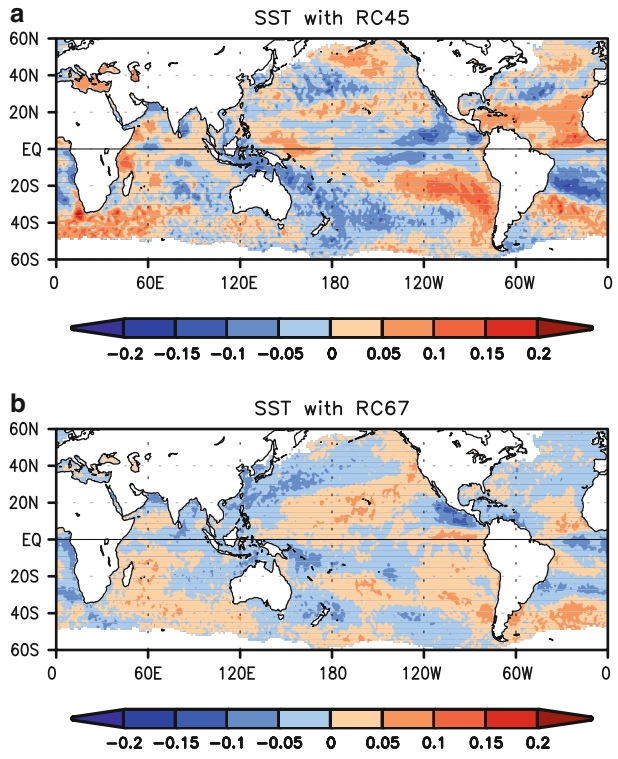

Fig. 10 Simultaneous point correlation of daily PC1 (shown in Fig. 3d, e) of **a** RC45 and **b** RC67 with daily SST anomalies during 1982–2007

the phase composites of mean sea level pressure (MSLP) and zonal wind u at several vertical levels based on the phases of RC45. These composites were computed in exactly the same manner as those of RC45 in Fig. 8a. For brevity, the composites of only the peak phases 2, 3, 6, and 7 are shown in Fig. 11a for MSLP and in Fig. 11b for u at 1000 hPa. The convective activities in phases 6 and 7 (Fig. 8a) are associated with low pressure between 40°N and 60°N in the North Atlantic and high pressure to the north of 60°N (Fig. 11a). Corresponding to these pressure systems, the composites of the zonal wind at 1,000 hPa have easterlies in the northern part and westerlies in the southern part of the North Atlantic (Fig. 11b). An examination of the composites of horizontal wind vectors (figure not shown) revealed anticyclonic circulation in the north and cyclonic circulation to the south. The same pressure and wind patterns with opposite sign are associated with suppressed convection in phases 2 and 3. These variations in pressure and lower level wind in the North Atlantic are quite similar to the variability and structure of the NAO.

The association of the intraseasonal oscillation with the MJO is explored by constructing phase composites of total OLR anomalies and zonal wind at 200 hPa, corresponding to the phase composites of RC67 in Fig. 8b. The composites of the total OLR anomalies for first half of the oscillatory cycle (phases 1–4) are shown in Fig. 12a. When the positive OLR anomalies develop over the southern part of the South American continent and over near Central America in phase 1, strong convection anomalies exist in the equatorial Indian Ocean and extend over the African continent. In phases 2 and 3, while the positive OLR anomalies become stronger over the SACZ and propagate to cover the African continent, the convection zone in the

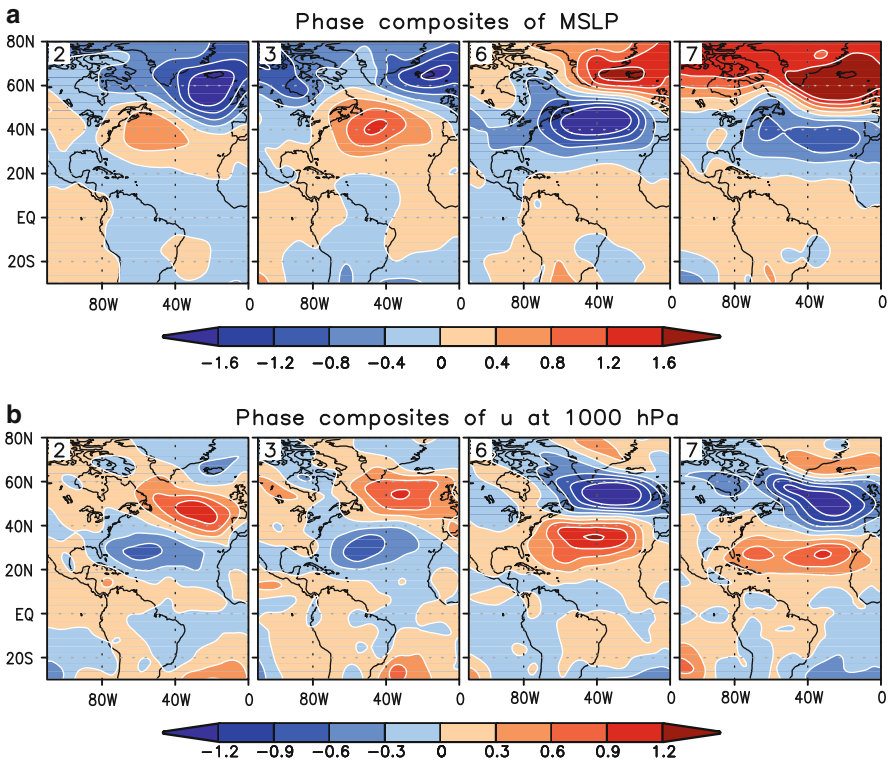

Fig. 11 Phase composites of daily **a** MSLP anomalies and **b** zonal wind (U) anomalies corresponding to four phase intervals (2, 3, 6 and 7) of the RC45 oscillatory mode during 1979–2007. Units are in hPa for MSLP and m s^{-1} for U. The phase interval number is given at the *top right corner* of each panel

Indian Ocean moves eastward into equatorial West Pacific Ocean. This convection center propagates further east in the Pacific Ocean and becomes weaker in phase 4 when the positive anomalies (suppressed convection) over the South American continent diminishes but moves eastward into the western Indian Ocean. This sequence is repeated with anomalies of opposite sign in phases 5–8 (figure not shown). Thus, there is a clear relation between the intraseasonal oscillation in the South American region and the MJO in the OLR composites.

Further support for this relation with the MJO is provided by similar phase composites of the zonal wind *u* at 200 hPa, as shown in Fig. 12b. In all the four phases shown in Fig. 12b, the convection center (Fig. 12a) is accompanied by easterlies to the west and westerlies to the east, indicating divergence at the top of the convection zone. The magnitude of the zonal wind also matches the intensity of the convection. It is noticeable that the westerlies in phases 3 and 4 flow over a large region extending from the East Pacific Ocean to the east coast of Africa and covering the entire northern part of the South American continent. The sequence in Fig. 12b is repeated in phases 5–8 with zonal wind anomalies in opposite directions (figure not shown). Similar composites of the zonal wind at a lower level were also examined (figure not shown). At the lower level, the convection zone is accompanied by westerlies to the west and easterlies to the east, indicating inflow and convergence into the convection center. These oscillatory patterns of convection and circulation anomalies basically describe the MJO cycle.

6.3 Regional variation

To find the regional variation of the two oscillations, the ARB and CESA indexes of RC45 (interseaseasonal) and RC67 (intraseasonal) are examined. For a better depiction of the daily variability, the time series of the two indexes are shown for a 10-year period covering 1981–1990 in Fig. 13. The amplitudes of ARB and CESA indexes of RC45 are comparable in the case of the interseasonal oscillation (Fig. 13a). However, the ARB index has slightly lower value and is almost 180° out of phase with the CESA index. In the case of the intraseasonal oscillation, the amplitude of the ARB index of RC67 is extremely small while the CESA index has considerable amplitude with pronounced modulation (Fig. 13b). Generally, the CESA index is more intense during the austral summer.

The DJFM seasonal mean of the ARB index is plotted in Fig. 14a for RC45 and RC67 showing that it is almost negligible for both the oscillations. In the case of CESA index, the DJFM seasonal mean of RC67 (intraseasonal) is almost negligible whereas the seasonal mean of RC45 (interseasonal) has small amplitude interannual variability (Fig. 14b).

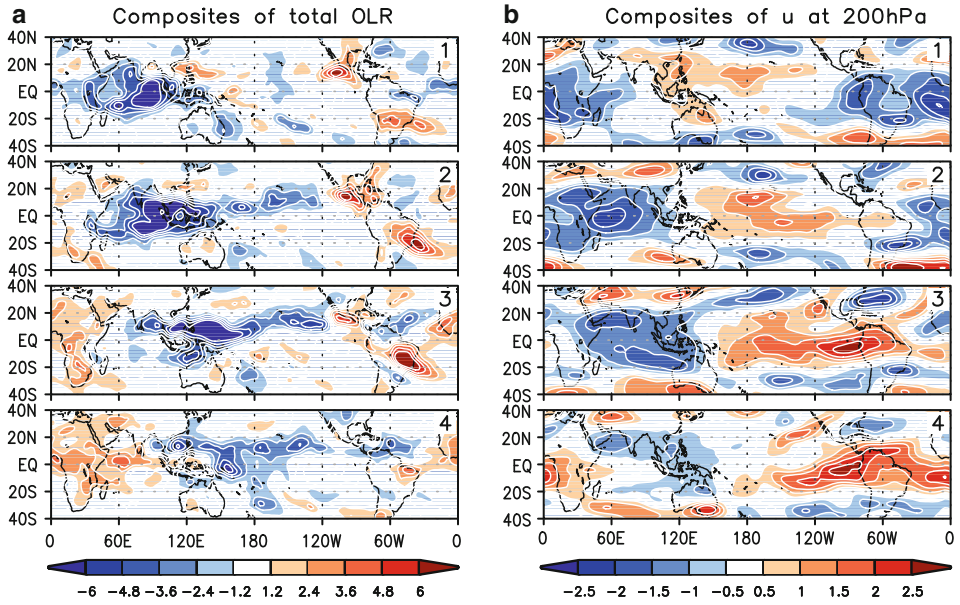

Fig. 12 Phase composites of **a** daily total OLR anomalies (*left panels*) **b** daily total zonal wind (u) anomalies at 200 hPa (*right panels*) corresponding to four phase intervals (1, 2, 3 and 4) of the RC67 oscillatory mode during 1979–2007. Units are in W m^{-2} for OLR and m s^{-1} for u. The phase interval number is given at the *top right corner* of each panel

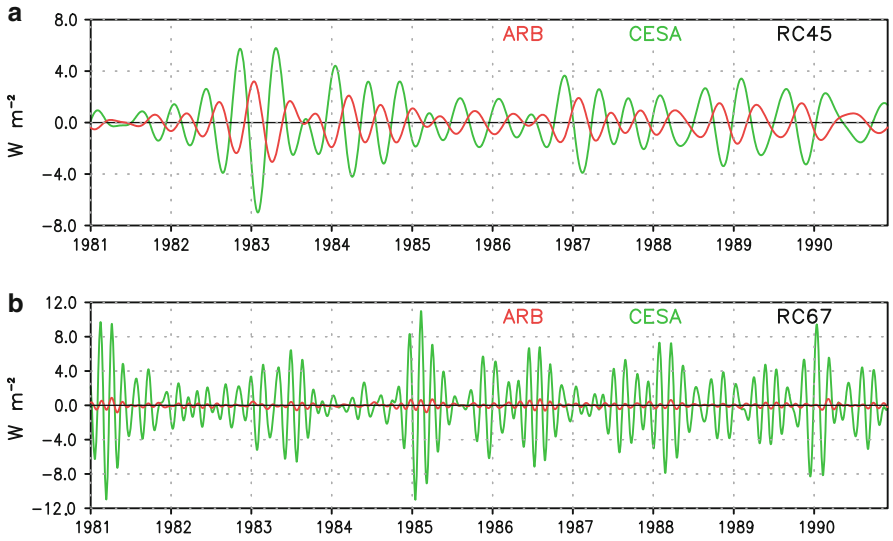

Fig. 13 Time series of ARB (*red*) and CESA (*green*) indexes of daily **a** RC45 and **b** RC67

The relative contributions of the two oscillations to the seasonal mean are examined by adding all the RCs from mode 1–7 (RC1+…+RC7) and computing the DJFM seasonal means of ARB and CESA indexes, as shown in Fig. 14c. Comparing with the seasonal means of RC123 in Fig. 7c, it is clear that the oscillatory modes do not contribute to the ARB index. However, the CESA index can be influenced by the interseasonal oscillation (RC45) to a small extent, as in the case of 1982, 1986, 1987 and 2005. Therefore, it suggests that the predictability of the seasonal mean rainfall is not affected by the intraseasonal variability.

7 Discussion

The observed daily OLR data were analyzed to determine the space–time structure of the daily atmospheric variability in the South American monsoon system. The main results indicate that three leading modes of daily variability are related to interannual and decadal phenomena such as ENSO, AMO and PDO. Additionally, there are two nonlinear oscillatory modes with periods in the interseasonal and intraseasonal time scales and indicate association with NAO and MJO, respectively. With the methodology adopted in this study, it was possible to obtain the daily

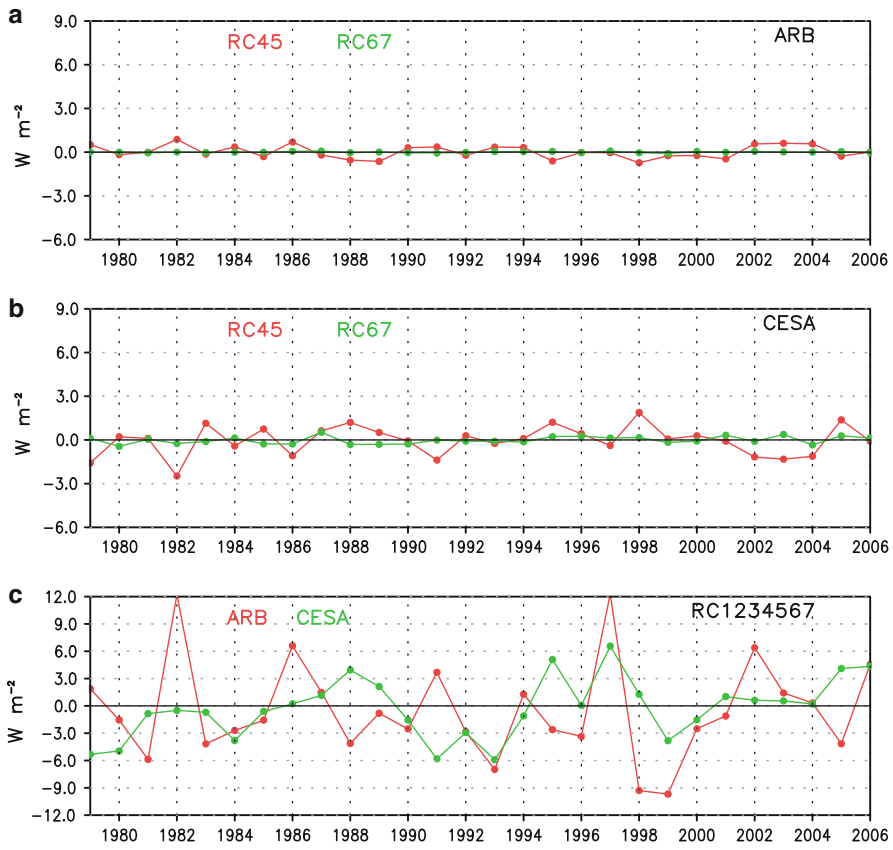

Fig. 14 Time series of **a** ARB and **b** CESA indexes of DJFM seasonal mean RC45 (*red*), RC67 (*green*). **c** Time series of ARB index (*red*) and CESA (*green*) of DJFM seasonal mean of RC1 + RC2 + RC3 + RC4 + RC5 + RC6 + RC7

variations of modes that have variability ranging from intraseasonal to decadal time scales. The association of the leading modes of SAMS in convection with various phenomena was established by examining the relation with daily anomalies of circulation fields and SST. It was also shown that the variability in two different regions (ARB and CESA) is similar for certain modes while there are differences in the magnitude and phase for the other modes.

The leading mode of daily variability has a broad spectral peak centered at about 4 years. The spatial structure of this mode consists of OLR anomalies of one sign over the northern part of the South American continent and the equatorial Atlantic Ocean and anomalies of opposite sign in the eastern Pacific Ocean and the southern part of the continent. This structure varies coherently according to the ENSO variability. The high correlation of this convection pattern with the Pacific SST and lower level winds provides strong support to its relation with the ENSO. The magnitude of this ENSO mode is found to be much higher in the ARB region than in the CESA region.

There are two modes (second and third MSSA modes) in the daily convection which reveal variability on decadal time scale. The relation with the daily SST and wind anomalies suggests that one of these patterns has a possible association with the AMO. The convection pattern of this mode consists of anomalies of same sign over the entire continent, extending well into the northern Atlantic Ocean. The amplitude of variability is almost the same in both ARB and CESA regions. Since the Atlantic Ocean has several modes of decadal variability, more evidence is needed to firmly establish the relation between the convection mode found in this study and the AMO. The other decadal mode of convection has anomalies of one sign over the northern part of the continent, eastern Pacific and northern Atlantic while anomalies of opposite sign exist in the southern part. The evidence for the association of this mode with the PDO is quite clear in the correlation pattern with the daily SST and in the regression pattern with the low level wind. For this mode, however, the variations in the ARB and CESA regions are opposite to each other with comparable magnitude.

Two nonlinear oscillations found in this study have periods of 165 days (interseasonal) and 52 days (intraseasonal) with broad-band spectra. Both the oscillations have similar spatial patterns in the SACZ region but different

patterns in the northern part and show northeastward propagation. The correlation with the daily SST is negligible for the two oscillations. However, the relations with the MSLP and horizontal winds provide evidence that the interseasonal oscillation is associated with the NAO. The evidence provided by the relations with other atmospheric fields suggests that the intraseasonal oscillation is part of the MJO. In the daily variability of the two oscillations, there are considerable differences between the ARB and CESA regions. In the interseasonal oscillation, the amplitudes in the ARB and CESA regions are comparable although the CESA region generally has higher values. The phase of this oscillation differs by almost 180° between the two regions. For the intraseasonal oscillation, however, the amplitude in the ARB region is almost negligible while it is quite high in the CESA region with pronounced seasonal modulation.

Despite the strong influences of ENSO and other SST related variability of the Pacific and Atlantic Oceans, the interannual variations in the SAMS can sometimes be subtle and also show quite different behavior in the ARB and CESA regions. The relative roles of the three low-frequency modes are important in determining the seasonal mean convection or precipitation during most years. The influence of ENSO can be either enhanced or reduced by the AMO or the PDO mode. For example, the influence of ENSO was enhanced in 1982 and 1997 while it was reduced (or counteracted) in 1991 for the ARB region. However, the ENSO influence in 1982 for the CESA region was counteracted by the AMO mode. During certain years, it is one of the decadal modes, rather than ENSO, that is important in determining the seasonal mean, such as during 1998 and 1999. Although the contribution of the interseasonal oscillation to the seasonal mean is small, it can matter in some years for the CESA region. For example, the ENSO influence in 1982 was further reduced by the interseasonal oscillation in the CESA region. The intraseasonal oscillation, on the other hand, does not seem to play a significant role in determining the seasonal mean monsoon. Still, because of its coherent nature and its regular time variability, the intraseasonal oscillation provides hope for better prediction on subseasonal time scale. The unified approach of this study in obtaining modes of longer time scales with strong relation to SST has provided strong support to Charney-Shukla hypothesis in the South American monsoon system also. A major implication of these results is that there is hope for long-term prediction of seasonal mean monsoon in the South American region. However, it is important to further understand the relative roles the Pacific and Atlantic Oceans.

Acknowledgments This research was supported by grants from the National Science Foundation (ATM-0332910, ATM-0830068), the National Oceanic and Atmospheric Administration (NA04OAR4310034, NA09OAR4310058, NA07OAR4310221), and the National Aeronautics and Space Administration (NNG04GG46G, NNX09AN50G). The authors thank Bohua Huang for helpful comments.

References

Aceitunuo P (1988) On the functioning of the southern oscillation in the south American sector part I: surface climate. Mon Wea Rev 116:505–524

Carvalho LMV, Jones C, Liebmann B (2002a) Extreme precipitation events in southeastern South America and large-scale convective patterns in the South Atlantic convergence zone. J Clim 15:2377–2394

Carvalho LMV, Jones C, Silva Dias MAF (2002b) Intraseasonal large-scale circulations and mesoscale convective activity in tropical South America during the TRMM-LBA campaign. J Geophys Res 107:D20. doi:10.1029/2001JD000745

Charney JG, Shukla J (1981) Predictability of monsoons. In: Lighthill J, Pearce RP (eds) Monsoon dynamics. Cambridge University Press, Cambridge, pp 99–109

Chaves RR, Nobre P (2004) Interactions between sea surface temperature over the South Atlantic ocean and the South Atlantic convergence zone. Geophys Res Lett 31:L03204. doi:10.1029/2003GL018647

Dettinger MD, Cayan DR, McCabe GJ, Marengo JA (2000) Multiscale streamflow variability associated with El Niño/Southern oscillation. In: Diaz HF, Markgraf V (eds) El Niño and Southern oscillation: multiscale variability and global and regional impacts. Cambridge University Press, Cambridge, pp 113–148

Doyle ME, Barros VR (2002) Midsummer low-level circulation and precipitation in subtropical South America and related sea surface temperature anomalies in the South Atlantic. J Clim 15:3394–3410

Fu R, Chen M, Li W, Dickinson RE (2001) How do tropical sea surface temperatures influence the seasonal distribution of precipitation in the equatorial Amazon? J Clim 14:4003–4026

Ghil M, Allen MR, Dettinger MD, Ide K, Kondrashov D, Mann ME, Robertson AE, Saunders A, Tian Y, Varadi F, Yiou P (2002) Advanced spectral methods for climatic time series. Rev Geophys 40(1):1003. doi:10.1029/2000RG000092

Grimm AM (2003) The El Niño impact on the summer monsoon in Brazil regional processes versus remote influences. J Clim 16:263–280

Grimm AM (2004) How do La Niña events disturb the summer monsoon system in Brazil? Clim Dyn 22:123–138

Grimm AM, Vera C, Mechoso CR (2005) The South American monsoon system. In: The global monsoon system: reasearch and forecast. World Meteorological Organization, Geneva. WMO/TD No. 1266:219–238

Huffman GJ, Adler RF, Morrissey M, Bolvin DT, Curtis S, Joyce R, McGavock B, Susskind J (2001) Global precipitation at one-degree daily resolution from multi-satellite observations. J Hydrometeor 2:36–50

Jones C, Carvalho LMV (2002) Active and break phases in the South American monsoon system. J Clim 15:905–914

Kanamitsu M, Ebisuzaki W, Woollen J, Yang S-K, Hnilo JJ, Fiorino M, Potter GL (2002) NCEP-DOE AMIP-II reanalysis (R-2). Bull Amer Meteorol Soc 83:1631–1643

Knight JR, Allan RJ, Folland CK, Vellinga M, Mann ME (2005) A signature of persistent natural thermohaline circulation cycles

in observed climate. Geophys Res Lett 32:L20708. doi: 10.1029/2005GL024233
Kousky VE, Kagano MT, Cavalcanti IFA (1984) A review of the Southern oscillation: ocean-atmospheric circulation changes and related rainfall anomalies. Tellus 36A:490–504
Krishnamurthy V, Kirtman BP (2009) Relation between Indian monsoon variability and SST. J Clim 22:4437–4458
Krishnamurthy V, Misra V (2010) Observed teleconnections with the South American monsoon system. Atmos Sci Lett 11:7–12
Krishnamurthy V, Shukla J (2007) Intraseasonal and seasonally persisting patterns of Indian monsoon rainfall. J Clim 20:3–20
Krishnamurthy V, Shukla J (2008) Seasonal persistence and propagation of intraseasonal patterns over the Indian monsoon region. Clim Dyn 30:353–369
Lenters JD, Cook KH (1997) On the origin of the bolivian high and related circulation features of the South American climate. J Atmos Sci 54:656–678
Liebmann B, Smith CA (1996) Description of a complete (interpolated) outgoing longwave radiation dataset. Bull Amer Soc 77:1275–1277
Liebmann B, Kiladis GN, Marengo JA, Ambrizzi T, Glick JD (1999) Submonthly convective variability over South America and the South Atlantic convergence zone. J Clim 12:1877–1891
Liebmann B, Jones C, Carvalho LMV (2001) Interannual variability of daily extreme precipitation events in the state of Sao Paulo, Brazil. J Clim 14:208–217
Mantua NJ, Hare SR, Zhang Y, Wallace JM, Francis RC (1997) A Pacific decadal climate oscillation with impacts on salmon production. Bull Amer Meteor Soc 78:1069–1079
Marengo JA (1992) Interannual variability of surface climate in the Amazon basin. Int J Climatol 12:853–863
Marengo JA (1995) Interannual variability of deep convection over the tropical South American sector as deuced from ISCCP C2 data. Int J Climatol 15:995–1010
Marengo JA, Hastenrath S (1993) Case studies of extreme climatic events in the Amazon basin. J Clim 6:617–627
Misra V (2008a) Coupled air sea and land interactions of the South American monsoon. J Clim 21:6389–6403
Misra V (2008b) Coupled interactions of the monsoons. Geophys Res Lett 35:L12705. doi:10.1029/2008GL033562
Moron V, Vautard R, Ghil M (1998) Trends interdecadal and interannual oscillations in global sea-surface temperatures. Clim Dyn 14:545–569
Nogués-Paegle J, Mo KC (1997) Alternating wet and dry conditions over South America during summer. Mon Wea Rev 125:279–291
Rao VB, Cavalcanti I, Hada K (1996) Annual variation of rainfall over Brazil and water vapor characteristics over South America. J Geophys Res 101:26359–26551
Reynolds RW, Smith TM, Liu C, Chelton DB, Casey KS, Schlax MG (2007) Daily high-resolution-blended analyses for sea surface temperature. J Clim 20:5473–5496
Robertson AW, Mechoso CR (2000) Interannual and interdecadal variability of the South Atlantic convergence zone. Mon Wea Rev 128:2947–2957
Robertson AW, Ferrara JD, Mechoso CR (2003) Simulations of the atmospheric response to South Atlantic sea surface temperature anomalies. J Clim 16:2540–2551
Ropelewski CF, Halpert MS (1987) Global and regional scale precipitation patterns associated with the El Niño/Southern oscillation. Mon Wea Rev 115:1606–1626
Vera C, Higgins W, Amador J, Ambrizzi T, Garreaud R, Gochis D, Gutzler D, Lettenmaier D, Marengo J, Mechoso CR, Nogues-Paegle J, Silva Dias PL, Zhang C (2006) Toward a unified view of the American monsoon systems. J Clim 19:4977–5000
Zhou J, Lau K-M (1998) Does a monsoon climate exist over South America? J Clim 11:1020–1040